JOURNAL OF AIRCRAFT
Vol. 38, No. 1, January–February 2001

Nonlinear Aeroelasticity and Flight Dynamics of High-Altitude Long-Endurance Aircraft

Mayuresh J. Patil* and Dewey H. Hodges†
Georgia Institute of Technology, Atlanta, Georgia 30332-0150
and
Carlos E. S. Cesnik‡
Massachusetts Institute of Technology, Cambridge, Massachusetts 02139

High-altitude long-endurance (HALE) aircraft have wings with high aspect ratios. During operations of these aircraft, the wings can undergo large static deflections. These large static deflections can change the natural frequencies of the wing, which, in turn, can produce significant changes in its aeroelastic behavior. This behavior can be accounted for only by using a rigorous nonlinear aeroelastic analysis. Results are obtained from such an analysis for aeroelastic behavior as well as overall flight dynamic characteristics of a complete aircraft model representative of HALE aircraft. When the nonlinear flexibility effects are taken into account in the calculation of trim and flight dynamics characteristics, the predicted aeroelastic behavior of the complete aircraft turns out to be very different from what it would be without such effects.

Introduction

HIGH-ALTITUDE long-endurance (HALE) aircraft have gained importance over the past decade. Unpiloted HALE aircraft are being designed for a variety of flight missions, including environmental sensing, military reconnaissance, and cellular telephone relay. HALE aircraft have high-aspect-ratio wings. To make the concept feasible in terms of weight restrictions, the wings are very flexible. Wing flexibility coupled with the long span leads to the possibility of large deflections during normal flight operation. Also, to fly at high altitudes and low speeds requires operation at high angles of attack, likely close to stall. Thus, it is unlikely that an aeroelastic analysis based on linearization about the undeformed wing could lead to accurate aeroelastic results. Even the trim condition and flight dynamic frequencies could be significantly affected by the flexibility and nonlinear deformation, which, in turn, could change the overall aeroelastic characteristics of the aircraft.

Research has been conducted in the past focusing on various areas comprising the problem just described. Nonlinear aeroelastic analysis has gathered a lot of momentum in the last decade due to the understanding of nonlinear dynamics as applied to complex systems and the availability of the required mathematical tools. The various studies evaluated the effect of aerodynamic stall nonlinearity, structural geometric nonlinearity, and free-play nonlinearity on the aeroelastic behavior of either an airfoil model or cantilevered wing model.

The studies conducted by Dunn and Dugundji are a combination of analysis and experimental validation of the effects of dynamic stall on aeroelastic instabilities for simple cantilevered laminated platelike wings.[1] The ONERA stall model was used for aerodynamic loads. Tang and Dowell have studied the flutter and forced response of a flexible rotor blade.[2] In the study, geometrical structural nonlinearity and free-play structural nonlinearity are taken into consideration. Again, high-angle-of-attack, unsteady aerodynamics was modeled using the ONERA dynamic stall model.

Virgin and Dowell have studied the nonlinear behavior of airfoils with control surface free play and investigated the limit-cycle oscillations and chaotic motion of airfoils.[3] Gilliatt et al. have investigated the nonlinear aeroelastic behavior of an airfoil experimentally and analytically.[4] A nonlinear support mechanism was constructed and is used to represent continuous structural nonlinearities.

The investigation of the effect of structural flexibility on the overall aeroelastic/flight dynamic behavior of an aircraft has been the topic of a few research efforts. Aeroelastic characteristics of highly flexible aircraft were investigated by van Schoor and von Flotow.[5] The complete aircraft was modeled using various modes of vibration, including rigid-body modes. The results indicate the need for inclusion of the aircraft flexibility in the flight dynamics analysis due to strong interactions between the low-frequency aeroelastic modes and flight dynamic modes. Linear aeroelastic and flight dynamic analysis results for a HALE aircraft are presented by Pendaries.[6] The results highlight the effect of rigid-body modes on wing aeroelastic characteristics and the effect of wing flexibility on the aircraft flight dynamic characteristics.

The present study presents the results obtained using a low-order, high-fidelity nonlinear aeroelastic analysis. A theoretical basis has been established for a consistent analysis that takes into account 1) material anisotropy, 2) geometrical nonlinearities of the structure, 3) unsteady flow behavior, 4) dynamic stall, and 5) rigid-body modes. The formulation and preliminary results for the nonlinear aeroelastic analysis of an aircraft have been presented in earlier papers.[7,8] The present paper extends previous work and presents results specific to HALE aircraft. The results obtained give insight into the effects of the structural geometric nonlinearities on the trim solution, flutter speed, and flight dynamic characteristics of a complete aircraft.

Present Model

The present theory is based on two separate models, namely, 1) a mixed variational formulation based on the exact intrinsic equations for dynamics of beams in moving frames[9] and 2) a finite-state airloads model for deformable airfoils on fixed and rotating wings.[10,11] The former theory is a nonlinear intrinsic formulation for the dynamics of initially curved and twisted beams in a moving frame. There are no approximations to the geometry of the reference line of the deformed beam or to the orientation of the cross-sectional reference frame of the deformed beam. A compact mixed variational formulation can be derived from these equations that is well suited

Presented as Paper 99-1470 at the 40th Structures, Structural Dynamics, and Materials Conference, St. Louis, MO, 12–15 April 1999; received 27 April 1999; revision received 7 August 2000; accepted for publication 28 August 2000.

*Graduate Research Assistant, School of Aerospace Engineering; currently Postdoctoral Fellow, School of Aerospace Engineering. Member AIAA.

†Professor, School of Aerospace Engineering. Fellow AIAA.

‡Assistant Professor, Aeronautics and Astronautics. Senior Member AIAA.

for low-order beam finite element analysis based in part on the original paper by Hodges.[9] The latter work presents a state-space theory for the lift, drag, and all generalized forces of a deformable airfoil. Trailing-edge flap deflections are included indirectly as a special case of generalized deformation. The model is based on thin-airfoil theory and allows for arbitrary small deformations of the airfoil fixed in a reference frame that can perform arbitrary large motions. A detailed formulation of the aeroelastic analysis of a complete aircraft is given in earlier papers by the authors.[7,8] Here, the theory is described briefly for the sake of completeness.

The equations of motion are derived using Hamilton's principle, given as,

$$\int_{t_1}^{t_2} [\delta(K - U) + \overline{\delta W}]\,\mathrm{d}t = \overline{\delta \mathcal{A}} \tag{1}$$

where K and U are the kinetic and potential (strain) energy, respectively; $\overline{\delta W}$ and $\overline{\delta \mathcal{A}}$ are the virtual work and virtual action terms; and t_1 and t_2 are the limits of the time interval over which the solution is required. The expressions of the kinetic energy and potential energy are derived using rigorous geometrically exact kinematics.[9] The virtual work is dependent on the applied forces, which, in the present case, are the unsteady aerodynamic forces obtained using the Peters airloads model (see Ref. 10). The inflow in the Peters airloads model is obtained using the finite-state inflow model (see Ref. 12).

By coupling the structural and aerodynamic models one obtains the complete aeroelastic model. By selecting the shape functions for the variational quantities in the formulation, one can choose between 1) finite elements in space and 2) finite elements in space and time. Using finite elements in space, one can obtain a set of ordinary nonlinear differential equations in time representing the equations of motion for the wing/aircraft. Coupling with the differential equations for the inflow leads one to a set nonlinear differential equations for the complete aeroelastic system. The steady-state solution can be calculated by solving the nonlinear algebraic equations obtained by removing the time-differentiated terms. One can then calculate linearized equations of motion about the steady state for stability analysis. Space–time finite elements can be used to discretize in space as well as time. By choosing only one element in time, one can obtain a set of nonlinear algebraic equations that can be used for time marching and, thus, to study the dynamic nonlinear behavior of the system. This kind of analysis is useful in investigating limit-cycle oscillations.

Thus, three kinds of solutions are possible: 1) a nonlinear steady-state solution, 2) a stability analysis for small motions about the steady state (by linearizing about the steady state), and 3) a time-marching solution for nonlinear dynamics of the system. The focus of the present paper is on the steady-state (trim) and stability calculations. The reader is refered to Ref. 13 for the time-marching solution and insight into the limit-cycle oscillations of the wing.

For steady-state and stability analyses, the formulation is converted to its weakest form in space, while retaining the time derivatives of variables. This is achieved by transferring the spatial derivatives of variables to the corresponding variation by integration by parts. Because of the formulation's weakest form, simple shape functions (linear) can be used.[9] With these shape functions, the spatial integration in a mixed variational equation can be performed explicitly to give a set of nonlinear equations.[14] These equations can be separated into structural (F_S) and aerodynamic (F_L) terms and written as

$$F_S(X, \dot{X}) - F_L(X, Y, \dot{X}) = 0 \tag{2}$$

where X are the structural degrees of freedom and Y are the inflow states. Similarly, one can separate the inflow equations into an inflow component, F_I, and a downwash component, F_W, as

$$-F_W(\dot{X}) + F_I(Y, \dot{Y}) = 0 \tag{3}$$

The solutions of interest for the two coupled sets of equations [Eqs. (2) and (3)] can be expressed in the form

$$\begin{Bmatrix} X \\ Y \end{Bmatrix} = \begin{Bmatrix} \bar{X} \\ \bar{Y} \end{Bmatrix} + \begin{Bmatrix} \check{X}(t) \\ \check{Y}(t) \end{Bmatrix} \tag{4}$$

where the overbar denotes steady-state values and the inverted carat denotes small perturbations about the steady state.

For the steady state, $\bar{Y}$ is identically equal to zero [from Eq. (3)]. Thus, one has to solve a set of nonlinear equations given by

$$F_S(\bar{X}, 0) - F_L(\bar{X}, 0, 0) = 0 \tag{5}$$

The Jacobian matrix of the preceding set of nonlinear equations can be obtained analytically and is found to be very sparse.[14] The steady-state solution can be found very efficiently using the Newton–Raphson method.

By perturbing Eqs. (2) and (3) about the calculated steady state [using Eq. (4)], one obtains the transient solution from

$$\begin{bmatrix} \dfrac{\partial F_S}{\partial \dot{X}} - \dfrac{\partial F_L}{\partial \dot{X}} & 0 \\ -\dfrac{\partial F_W}{\partial \dot{X}} & \dfrac{\partial F_I}{\partial \dot{Y}} \end{bmatrix}_{\substack{X=\bar{X} \\ Y=0}} \begin{Bmatrix} \dot{\check{X}} \\ \dot{\check{Y}} \end{Bmatrix} + \begin{bmatrix} \dfrac{\partial F_S}{\partial X} - \dfrac{\partial F_L}{\partial X} & -\dfrac{\partial F_L}{\partial Y} \\ 0 & \dfrac{\partial F_I}{\partial Y} \end{bmatrix}_{\substack{X=\bar{X} \\ Y=0}} \begin{Bmatrix} \check{X} \\ \check{Y} \end{Bmatrix} = \begin{Bmatrix} 0 \\ 0 \end{Bmatrix} \tag{6}$$

Now, assuming the perturbational quantities to be proportional to e^{st}, one can solve the preceding equations as an eigenvalue problem to get the modal damping, frequency, and mode shape of the various modes. The stability condition of the aeroelastic system at various operating conditions is thus obtained.

Results

Table 1 gives the structural and planform data for the aircraft model under investigation. The aircraft model has very high-aspect-ratio wings (see Fig. 1) and is geometrically similar to HALE aircraft. In the next section, linear structural dynamics and aeroelasticity results will be presented and compared with results obtained using linear modal analysis. Next, results with nonlinearities included are presented to show their importance. These include natural frequencies, flutter frequencies and speeds, and loci of roots, all

Table 1 Aircraft model data

Parameter	Value
Wing	
Half span	16 m
Chord	1 m
Mass per unit length	0.75 kg/m
Moment of inertia (50% chord)	0.1 kg · m
Spanwise elastic axis	50% chord
Center of gravity	50% chord
Bending rigidity	2×10^4 N · m^2
Torsional rigidity	1×10^4 N · m^2
Bending rigidity (chordwise)	4×10^6 N · m^2
Payload and tailboom	
Mass	50 kg
Moment of inertia	200 kg · m^2
Length of tail boom	10 m
Tail	
Half-span	2.5 m
Chord	0.5 m
Mass per unit length	0.08 kg/m
Moment of inertia	0.01 kg · m
Center of gravity	Midchord
Flight condition	
Altitude	20 km
Density of air	0.0889 kg/m^3

Table 2 Comparison of linear frequency results (rad/s)

Mode	Present analysis	Exact	% Error
First flatwise bending	2.247	2.243	+0.2
Second flatwise bending	14.606	14.056	+3.9
Third flatwise bending	44.012	39.356	+11.8
First torsion	31.146	31.046	+0.3
First edgewise bending	31.739	31.718	+0.1

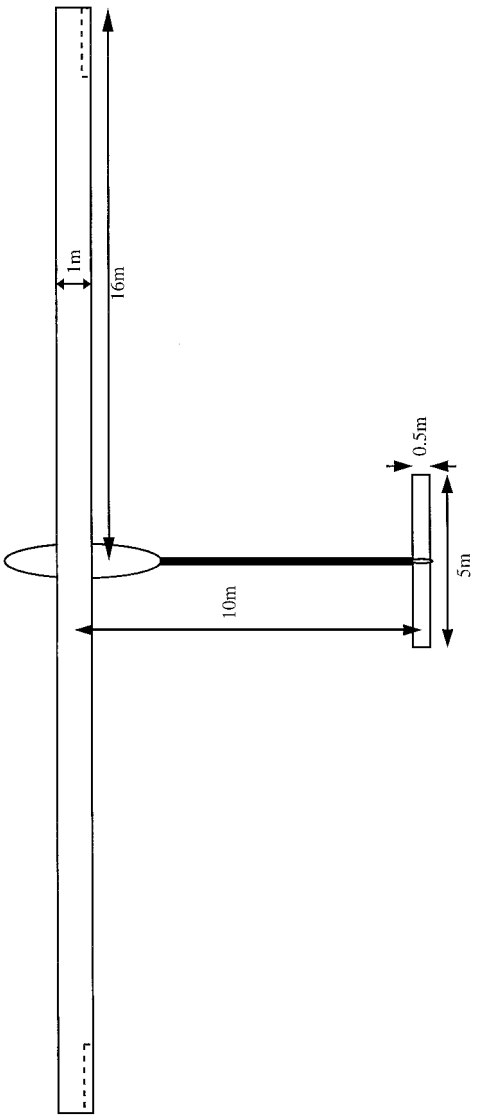

Fig. 1 Aircraft model geometry.

obtained for an analysis linearized about an equilibrium configuration calculated from a fully nonlinear analysis.

Linear Results

Table 2 presents frequency results based on theories that are linearized about the undeformed state, that is, the usual linear approach. The results for the present wing model were obtained using eight finite elements with all nonlinear effects suppressed. They are compared with the exact frequencies of a beam. The frequencies are very close except for the third flatwise bending mode. The inaccuracy of the third flatwise bending mode can be attributed to the coarse finite elements discretization (eight elements); however, the third flatwise bending mode does not significantly influence the aeroelastic results for this particular example.

Table 3 presents results from a linear calculation for flutter frequency and speed for the present wing model. The results from the present analysis are obtained with all nonlinear effects suppressed.

Table 3 Comparison of linear aeroelastic results

Parameter	Present analysis	Analysis of Ref. 15	% Difference
Flutter speed, m/s	32.21	32.51	−0.9
Flutter frequency, rad/s	22.61	22.37	+1.1
Divergence speed, m/s	37.29	37.15	+0.4

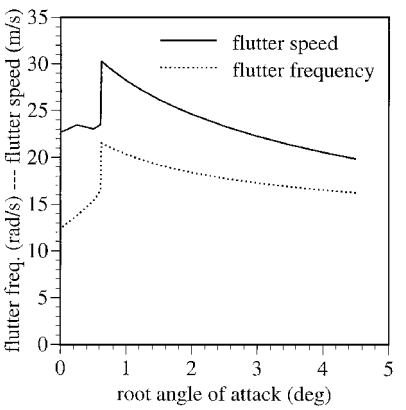

Fig. 2 Variation of flutter speed with angle of attack.

Eight finite elements are used to model the structure and six inflow states are used to model the inflow within each of the finite elements. The results are compared against those obtained using the theory of Ref. 15, which uses a Rayleigh–Ritz structural analysis with uncoupled beam mode shapes and Theodorsen's two-dimensional thin-airfoil theory for unsteady aerodynamics. The results are practically identical, indicating that eight finite elements are sufficient for the purposes of aeroelastic flutter calculations.

Nonlinear Flutter Results

What is meant by nonlinear flutter needs to be clarified. First, the complete nonlinear model is used to obtain the static equilibrium configuration. Then, the equations are dynamically linearized about the static equilibrium configuration to obtain a set of linear differential equations in terms of the perturbation variables. Flutter analysis is then conducted with these linearized equations of motion to calculate the nonlinear flutter speed.

Results are first presented for just the wing (with a cantilevered boundary condition). To investigate the effect of flight loads, the analysis is conducted for various values of angle of attack. The proper angle of attack in flight will be a function of the flight configuration. Figure 2 presents the nonlinear flutter results for the wing model including static deformation due to gravity and aerodynamic forces. The flutter speed and frequency at each value of root angle of attack is obtained as follows: 1) choose a flight speed, 2) calculate the static equilibrium deformed shape at the flight speed, 3) dynamically linearize about the deformed shape, 4) calculate the eigenvalues of the linearized system, 5) check for stability, if stable, increase the flight speed and repeat all of the preceding steps until instability speed is reached.

Figure 2 shows the variation of the nonlinear flutter speed as a function of α_0, the root angle of attack. The plot shows rapid changes in the flutter speed at low values of α_0. Also, the nonlinear flutter speed and frequency are much lower than those estimated by the linear model. At low α_0, the aerodynamic forces are low and gravitational forces lead to downward bending of the wing. As will be explained in detail in the next section, wing bending leads to structural nonlinearities, which, in turn, change the aeroelastic characteristics of the wing. At around 0.61 deg, there is a jump in the flutter speed and frequency. After the jump there is a smooth decrease in flutter speed and frequency. At around 4.5 deg, the flutter speed again jumps, this time off of the scale of the plot. Figure 3 shows the corresponding tip displacement at the flutter speed. As expected, the tip displacement is negative for low α_0. There is a discontinuity in the tip displacement that coincides with the discontinuity in

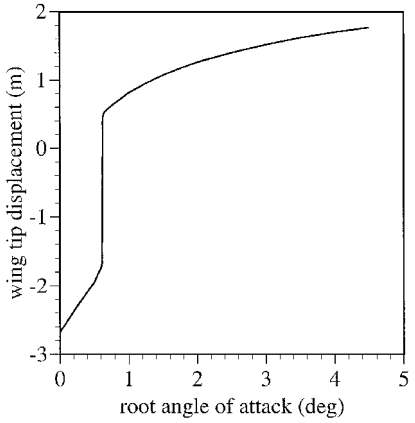

Fig. 3 Flutter static tip displacement at various root angles of attack.

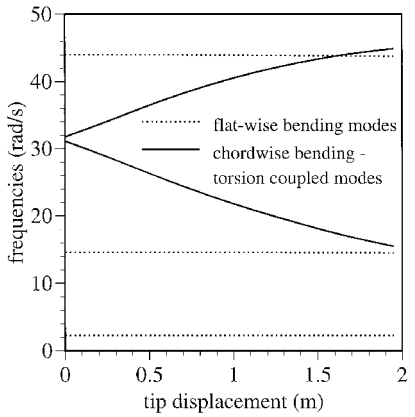

Fig. 4 Variation of structural frequencies with tip displacement.

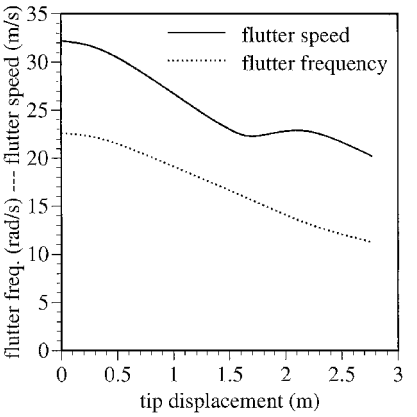

Fig. 5 Variation of flutter speed and frequency with given static tip displacement.

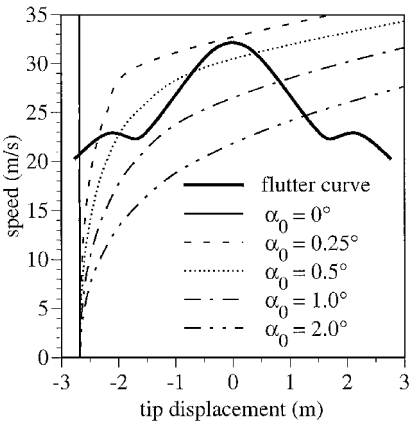

Fig. 6 Correlation of flutter speed and wing tip displacement.

flutter speed and frequency in Fig. 2. After the discontinuity, the tip displacement increases monotonically. Note that in actual 1-*g* flight, α_0 will be high enough so that the lift balances the weight of both the wing and fuselage, and, thus, the deformed wing shape will always be curved upward. Comparing the two plots, one can infer that wing bending (or tip displacement) is favorable for flutter and leads to decrease in the flutter speed.

Flutter Speed and Tip Displacement

It turns out that there is a strong relationship between the wing-tip displacement and the flutter speed. In the example considered, the drastic change in aeroelastic characteristics is due to changes in the structural characteristics of the wing due to bending (tip displacement). Unfortunately, this effect is easily confused with that due to additional velocity-tip displacement coupling introduced by α_0, that is, apart from flutter speed being a function of tip displacement (due to structural nonlinearities), the tip displacement itself is a function of the speed (due to aerodynamic forces, which are a function of speed).

The case study presented in this section uses a tip load to deform the wing. This tip load is not a function of flight speed, and one can clearly observe the effect of bending on the wing flutter. First, the results for the variation of structural natural frequencies as a function of wing-tip displacement are shown in Fig. 4. Structural deformation in wing bending (up and down or flatwise) leads to coupling between the torsion and edgewise bending mode. This coupling can be physically understood by observing that an edgewise force on a deformed wing would lead to twisting. The reader is referred to Ref. 16 for details. In the present case, one observes a large decrease in the modal frequency for the torsion mode (which becomes coupled torsion/edgewise bending mode) as tip displacement is increased. The flatwise bending modes are unaffected. Figure 5 shows the corresponding drop in both flutter speed and flutter frequency with increase in tip displacement. This decrease in the flutter speed (and frequency) is directly connected to the decrease in the torsional frequency with deformation. Lower torsional frequency helps in coupling with the flatwise bending mode, leading to lower flutter speed.[17]

To understand the results presented in the previous section, one needs now to do some cross plotting. Figure 6 demonstrates how closely the wing-tip displacement correlates with the flutter speed, and how it could be used to obtain flutter results for various values of α_0 (as presented in Fig. 2). The thick line plots the flutter speed as a function of tip displacement (same as Fig. 5). The other curves plot the tip displacement as a function of speed at various α_0. For example, the solid line for $\alpha_0 = 0$ deg is just a straight line because the tip displacement is only due to gravity. For very small α_0, the flutter and tip displacement curves intersect at very small speeds, and one gets very low flutter speeds. For slightly higher α_0, around 0.5 deg, the flutter and tip displacement curves intersect three times. Thus, one observes that the wing flutters in a range of speeds, after which it is again stable for a range of speeds, after which it flutters again. The range of speeds over which the wing flutters, however, decreases with increasing α_0. At around $\alpha_0 = 0.75$ deg, the first two intersection points collapse, the first range of flutter speed disappears, and the flutter speed jumps to the next flutter range. At this α_0, one sees a jump in the flutter speed from approximately 22 m/s up to about 28 m/s, and a corresponding jump in the tip displacement.

In summary, the nonlinear effects related to flutter (for the present model) are associated with the shift in natural frequencies caused by the change in static equilibrium configuration. This explains the decrease in the flutter speed shown in Fig. 2. Figure 6 gives more insight into the behavior of the system and provides a complete picture of the range and strength of instability and the existence of hump modes (small regions of weak instability).

The jump in flutter speed at $\alpha_0 = 4.5$ deg (Fig. 2) can also be explained by similar matching. Figure 7 shows the frequency and damping plots for larger angles of attack. Again, flutter occurs in

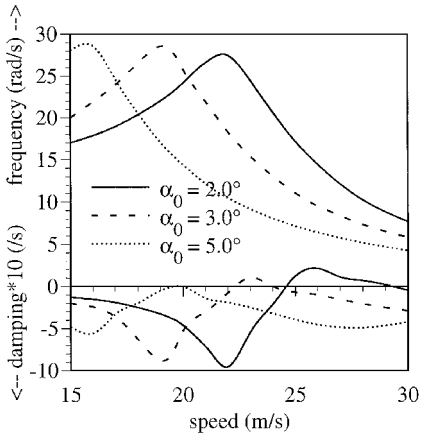

Fig. 7 Frequency and damping plots for various root angles of attack.

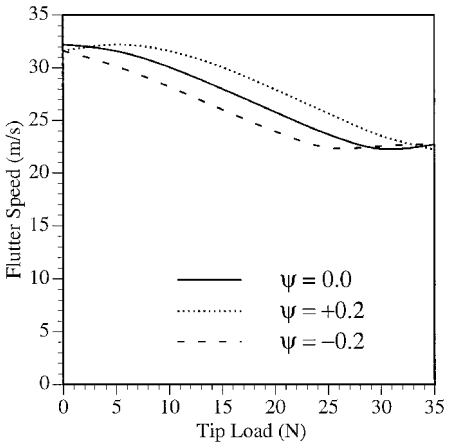

Fig. 8 Effect of torsion/edgewise bending structural coupling on the nonlinear flutter results.

a small range above the flutter critical speed. Though the flutter speed is decreasing with α_0, the strength and range of flutter is also decreasing. At around 4.5 deg, the damping does not reach zero before reversing its direction and increasing; thus, there is a jump in flutter speed. Note here that even though there is no instability, the damping at some flight speeds may be very close to zero, possibly leading to large vibrations.

Avoiding Deleterious Nonlinear Effects

As discussed in the earlier section, lift-induced curvature of the beam leads to a significant decrease in the flutter speed. This degradation of the aeroelastic characteristics can be attributed to coupling between torsion and edgewise bending, induced by that curvature. Thus, one could possibly increase the flutter speed by applying an opposite coupling.

Figure 8 shows the effect of structural coupling on the nonlinear aeroelastic characteristics of the wing. The parameter ψ is the cross-sectional coupling coefficient defined by the ratio of the torsion/edgewise bending coupling flexibility to the square root of the product of the torsional and edgewise bending flexibility. It is assumed that a maximum coupling of ± 0.2 can be obtained by structural tailoring. As seen in Fig. 8, the coupling leads to shift of the flutter speed. One can thus obtain an approximately 10% increase in the flutter speed with such induced coupling.

To increase the flutter speed at a specific loading condition, one could precurve the wing downward so that at the nominal flight condition the wing is approximately straight. Figure 9 shows the effect of precurvature on the nonlinear flutter results. Note that one could tailor the curvature so that at the trim condition, the wing is almost straight, and, thus, the flutter speed will be increased to a level close to the undeformed wing flutter speed. Note that the

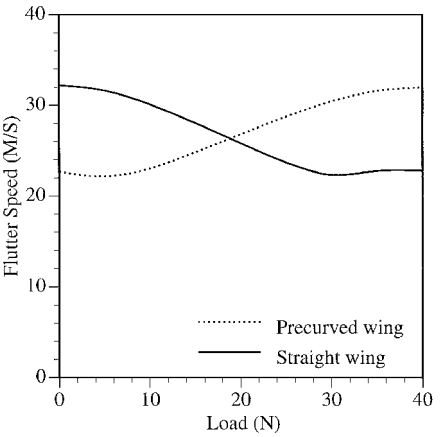

Fig. 9 Effect of precurvature on the nonlinear flutter results.

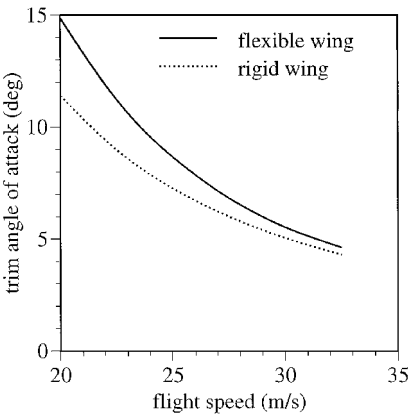

Fig. 10 Variation of $\bar{\alpha}_0$ with flight speed.

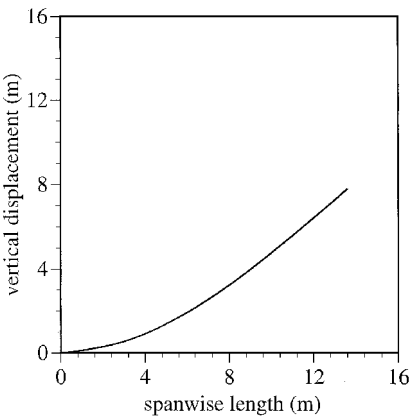

Fig. 11 Wing displacement at 25 m/s.

downward precurvature is limited by the ground clearance required of the wings.

Trim Results

This section investigates the static trim results for the airplane. Figure 10 shows the trim angle of attack $\bar{\alpha}_0$ at various flight speeds. Here, $\bar{\alpha}_0$ is obtained by calculating the angle of attack that gives the required vertical force. Contrary to expectations based only on linear static aeroelasticity, the value of $\bar{\alpha}_0$ required from a flexible wing is more than that from a rigid one. This is because the aerodynamic lift is directed at an angle perpendicular to the flow and the wing reference line, which, in the present case of large flatwise bending, implies that the lift does not act in the vertical direction. The displacement along the wing is certainly outside the region of applicability of linear theory, as indicated in Fig. 11, which shows the displacement shape of the wing at a 25 m/s forward speed trim condition. This large deformation and associated loss of aerodynamic

Table 4 Comparison of rigid aircraft flight dynamics

Parameter	Present analysis	Analysis of ref. 18	% Difference
Phugoid frequency ω_{n_P}	0.320	0.319	+0.3
Phugoid damping ζ_P	0.0702	0.0709	−1.0
Short period frequency $\omega_{n_{SP}}$	5.47	5.67	−3.5
Short period damping ζ_{SP}	0.910	0.905	+0.6

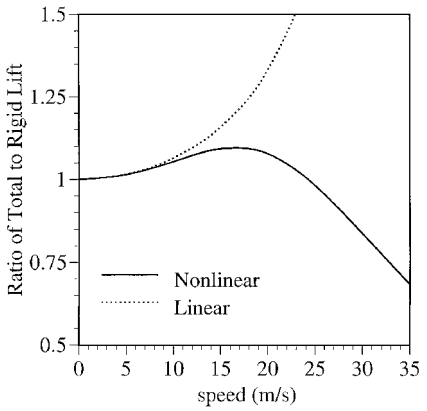

Fig. 12 Total lift to rigid lift ratio at $\alpha_0 = 5$ deg.

force in the vertical direction leads to the requirement of a higher value of $\bar{\alpha}_0$.

Figure 12 plots the ratio of total lift (force in vertical direction perpendicularto the flight velocity and span) to rigid lift as a function of speed. The drastic loss of effective vertical lift is clearly observed in the nonlinear model as compared to the linear one. The main significance of this result lies in that, if the stall angle is around 10 deg, then the rigid-wing analysis gives the stall speed to be 22 m/s, whereas the actual flexible aircraft would stall at a higher flight speed of around 25 m/s (see Fig. 10). The use of linear theory to predict aircraft performance would, thus, lead to incorrect estimation of the flight envelope.

Rigid Aircraft Flight Dynamics

Table 4 shows the phugoid and short-period mode results for the example aircraft flying at 25 m/s. The results are obtained given a rigid wing and are compared against the frequencies obtained by a simple rigid aircraft analysis given by Roskam.[18] One sees that results from the present analysis are essentially identical to the previously published results.

Stability of Complete Aircraft

When flexibility effects are taken into account in a flight dynamic analysis, the behavior is distinctly different from that of a rigid aircraft. Figure 13 compares the flight dynamics roots (frequencies and dampings) obtained with and without wing flexibility. The phugoid as well as the short-period mode are affected by wing flexibility. To see the transition of the root locus plot from rigid aircraft to flexible aircraft, a stiffened aircraft root locus plot is also provided. The stiffened aircraft wing stiffnesses are five times the actual wing stiffnesses. With the help of this additional case, the drastic difference in the flight dynamic modes due to wing flexibility can be seen as a smooth transition rather than a jump.

On the other hand, the rigid-body modes usually associated with the flight dynamic roots also affect the aeroelastic behavior of the wing. Figure 14 compares the root locus plot for the complete aircraft (including nonlinear aeroelastic analysis and rigid-body modes) with those obtained by using linear wing aeroelastic analysis and nonlinear wing aeroelastic analysis. The nonlinear wing aeroelastic analysis uses the known flight trim angle of attack as the equilibrium condition, and the eigenvalue analysis is conducted at that steady state. A magnified plot is inserted that shows the qualitative differences in more detail. Clearly, the low-frequency modes that in-

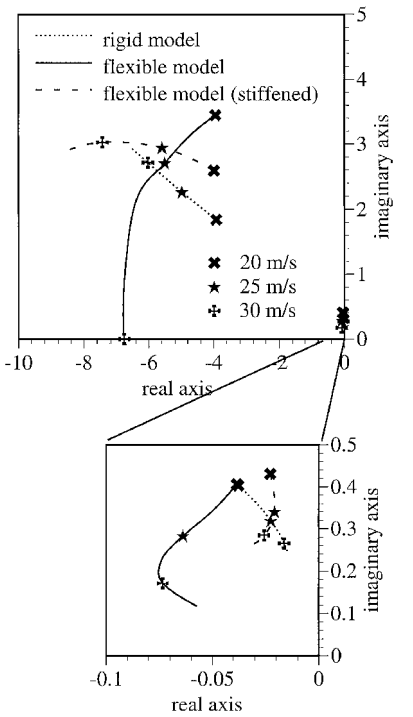

Fig. 13 Root locus plot showing the flight dynamics roots, with a magnified section showing the roots nearest the origin.

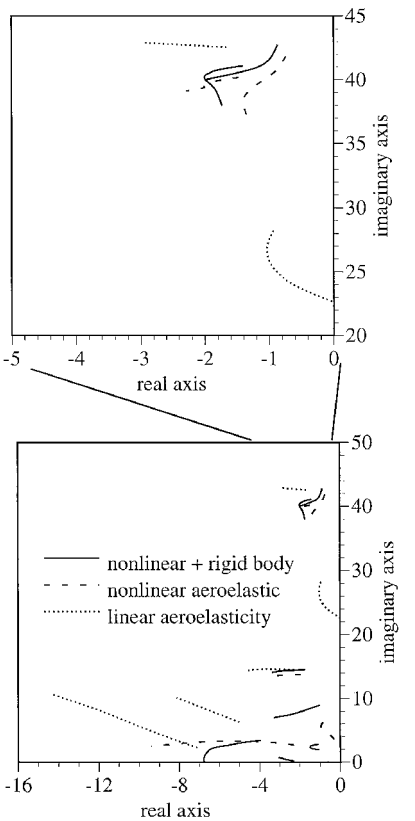

Fig. 14 Expanded root locus plot with magnified section inserted that depicts roots in vicinity of the unstable root.

volve wing flexibility are completely coupled to the flight dynamic modes, changing their behavior completely. On the other hand, the high-frequency wing aeroelastic modes do not strongly couple with the flight dynamic modes. However, the effect of the trim condition is very important because the trim condition defines the nonlinear equilibrium about which the aeroelastic model is dynamically linearized. Thus, the flutter modes are not predicted accurately by the linear theory, but the nonlinear wing theory does a good job

because the flutter modes are primarily affected by the wing structural nonlinearity. Thus, if the static trim solution is properly taken into account, one can expect a simplified nonlinear analysis, for example, one that includes only the cantilevered wing, to give a good estimate of the complete aircraft aeroelastic stability.

Conclusions

A nonlinear aeroelastic study has been conducted on a complete aircraft model geometrically similar to current HALE aircraft. Because of the large aspect ratio of the wing, the corresponding large deflections under aerodynamic loads, and the changes in the aerodynamic loads due to the large deflections, there can be significant changes in the aeroelastic behavior of the wing. In particular, significant changes can occur in the natural frequencies of the wing as a function of its tip displacement that very closely track the changes in the flutter speed. This behavior can be accounted for only by using a rigorous nonlinear aeroelastic analysis. The reduction in flutter speed due to the nonlinear coupling among edgewise wing bending and torsion (arising from the flatwise bending deformation) can be decreased by the introduction of opposite structural coupling between torsion and edgewise bending, for example, by the use of composite tailoring, or it could be effectively eliminated by precurving the wing.

The overall flight dynamic characteristics of the aircraft also change due to wing flexibility. In particular, the trim solution as well as the short-period and phugoid modes are affected by wing flexibility. Should one neglect the nonlinear trim solution and the flight dynamic frequencies, one may find the predicted aeroelastic behavior of the complete aircraft to be very different from its actual behavior.

Acknowledgments

This work was supported by the U.S. Air Force Office of Scientific Research (Grant F49620-98-1-0032). The Technical Monitor was Brian P. Sanders.

References

[1]Dunn, P., and Dugundji, J., "Nonlinear Stall Flutter and Divergence Analysis of Cantilevered Graphite/Epoxy Wings," *AIAA Journal*, Vol. 30, No. 1, 1992, pp. 153–162.

[2]Tang, D. M., and Dowell, E. H., "Experimental and Theoretical Study for Nonlinear Aeroelastic Behavior of a Flexible Rotor Blade," *AIAA Journal*, Vol. 31, No. 6, 1993, pp. 1133–1142.

[3]Virgin, L. N., and Dowell, E. H., "Nonlinear Aeroelasticity and Chaos," *Computational Nonlinear Mechanics in Aerospace Engineering*, edited by S. N. Atluri, AIAA, Washington, DC, 1992, Chap. 15.

[4]Gilliatt, H. C., Strganac, T. W., and Kurdila, A. J., "Nonlinear Aeroelastic Response of an Airfoil," *Proceedings of the 35th Aerospace Sciences Meeting and Exhibit*, AIAA Paper 97-0459, Reston, VA, 1997.

[5]van Schoor, M. C., and von Flotow, A. H., "Aeroelastic Characteristics of a Highly Flexible Aircraft," *Journal of Aircraft*, Vol. 27, No. 10, 1990, pp. 901–908.

[6]Pendaries, C., "From the HALE Gnopter to the Ornithopter—or How to Take Advantage of Aircraft Flexibility," *Proceedings of the 21st Congress of the International Council of the Aeronautical Sciences*, AIAA Paper A98-31715, Reston, VA, 1998.

[7]Patil, M. J., Hodges, D. H., and Cesnik, C. E. S., "Nonlinear Aeroelastic Analysis of Aircraft with High-Aspect-Ratio Wings," *Proceedings of the 39th Structures, Structural Dynamics, and Materials Conference*, AIAA, Reston, VA, 1998, pp. 2056–2068.

[8]Patil, M. J., Hodges, D. H., and Cesnik, C. E. S., "Nonlinear Aeroelastic Analysis of Complete Aircraft in Subsonic Flow," *Journal of Aircraft*, Vol. 37, No. 5, 2000, pp. 753–760.

[9]Hodges, D. H., "A Mixed Variational Formulation Based on Exact Intrinsic Equations for Dynamics of Moving Beams," *International Journal of Solids and Structures*, Vol. 26, No. 11, 1990, pp. 1253–1273.

[10]Peters, D. A., and Johnson, M. J., "Finite-State Airloads for Deformable Airfoils on Fixed and Rotating Wings," *Symposium on Aeroelasticity and Fluid/Structure Interaction, Proceedings of the Winter Annual Meeting*, AD Vol. 44, American Society of Mechanical Engineers, Fairfield, NJ, 1994, pp. 1–28.

[11]Peters, D. A., Barwey, D., and Johnson, M. J., "Finite-State Airloads Modeling with Compressibility and Unsteady Free-Stream," *Proceedings of the Sixth International Workshop on Dynamics and Aeroelastic Stability Modeling of Rotorcraft Systems*, U.S. Army Research Office, 1995.

[12]Peters, D. A., Karunamoorthy, S., and Cao, W.-M., "Finite State Induced Flow Models; Part I: Two-Dimensional Thin Airfoils," *Journal of Aircraft*, Vol. 32, No. 2, 1995, pp. 313–322.

[13]Patil, M. J., Hodges, D. H., and Cesnik, C. E. S., "Limit Cycle Oscillations in High-Aspect-Ratio Wings," *Journal of Fluids and Structures* (to be published).

[14]Hodges, D. H., Shang, X., and Cesnik, C. E. S., "Finite Element Solution of Nonlinear Intrinsic Equations for Curved Composite Beams," *Journal of the American Helicopter Society*, Vol. 41, No. 4, 1996, pp. 313–321.

[15]Patil, M. J., "Aeroelastic Tailoring of Composite Box Beams," *Proceedings of the 35th Aerospace Sciences Meeting and Exhibit*, AIAA Paper 97-0015, Reston, VA, 1997.

[16]Minguet, P., and Dugundji, J., "Experiments and Analysis for Composite Blades Under Large Deflections. Part II: Dynamic Behavior," *AIAA Journal*, Vol. 28, No. 9, 1990, pp. 1580–1588.

[17]Patil, M. J., Hodges, D. H., and Cesnik, C. E. S., "Characterizing the Effects of Geometrical Nonlinearities on Aeroelastic Behavior of High-Aspect-Ratio Wings," NASA CP 1999/209136, 1999.

[18]Roskam, J., *Airplane Flight Dynamics and Automatic Flight Controls*, Roskam Aviation and Engineering Corp., Ottawa, KS, 1979, Chap. 6.